ID 159

Structural Analysis of a Bearingless Rotor System using an Improved Flexible Multi-body Model

TaeYoung Chun and SangJoon Shin
School of Mechanical and Aerospace Engineering, Seoul National University
599 Gwanak-ro, Gwanak-gu, Seoul 151-742, Republic of Korea
and
YoungJung Kee
Korea Aerospace Research Institute, Daejeon 305-333, Republic of Korea

This paper presents an improved finite element analysis for a bearingless helicopter rotor. A bearingless rotor system consists of the following three major components: a main rotor blade, a wrap-around torque tube, and flexbeams. Since the bearingless rotor features a significantly large elastic twist in the flexbeam and additional unique structural characteristics, it contains significant structural nonlinearity and redundancy between bending and torsion. Thus, it requires sophisticated structural modeling and relevant numerical prediction because of its multiple load paths, which is induced by the single or multiple flexbeams and torque tube.

In this paper, based on Hamilton's principle, finite element formulation is used to allow the multiple sub-components to be considered as beam elements individually. Geometrically exact beam formulation is used to construct the finite element model to consider the nonlinear characteristics precisely and estimate an aeromechanical behavior. To enforce the kinematic constraint between structural models, Lagrange's multiplier is used. In this way, multi-body modeling of the bearingless rotor will be enabled.

1. Introduction

This paper presents an improved finite element analysis for a bearingless helicopter rotor. A bearingless rotor system consists of the following three major components: a main rotor blade, a wrap-around torque tube, and flexbeams. Instead of a conventional pitch bearing, it adopts a torsionally-soft flexbeam, which is located between the main blade and hub. Because the bearingless rotor features a significantly large elastic twist in the flexbeam and additional unique structural characteristics, it contains significant structural nonlinearity and redundancy between bending and torsion. Thus, it requires sophisticated structural modeling and relevant numerical prediction because of its multiple load paths, which is induced by single or multiple flexbeams and torque tube.

Fig. 1 shows main components of a bearingless rotor system. Those are rotor blade, single or multiple flexbeams, torque tube, lead-lag damper and hub plate. The distinguishing features of the bearingless rotor are a torsionally-soft flexbeam and a torsionally-stiff torque tube. Due to elastic deformation of the flexbeams the role of structural hinge is implemented. A torsionally stiff torque tube, which is soft in bending, is used to transmit the pitch control torque to the outboard end of the flexbeam. Flexbeams, torque tube, and rotor blade are connected by a relatively rigid clevis.

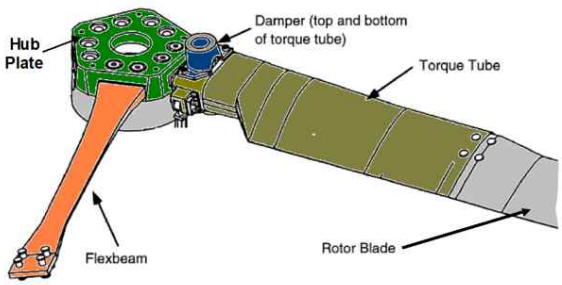

Fig. 1 Bearingless rotor blade configuration

In the literature, a few attempts to analyze a bearingless rotor have been reported. Hodges [1] modeled the bearingless rotor system consisting of a flexbeam and a torque tube using the moderate deflection type beam theory. Hong and Chopra [2] performed aeroelastic analysis of an I-section flexbeam model in hover. Sivaneri and Chopra [3, 4] modeled a bearingless rotor including two flexbeams. And existing programs such as University of Maryland Advanced Rotorcraft Code (UMARC) [5] and the Comprehensive Analytical Model of Rotorcraft Aerodynamics and

Dynamics (CAMRAD II) [6] have been widely used to analyze a bearingless rotor system.

UMARC uses a geometrically nonlinear but approximated beam formulation, which only retains the terms up to the second order based on an ordering scheme [7]. CAMRAD II provides an exact beam model regarding the geometrical non-linearity. However, it requires a significant amount of detailed input parameters in order to obtain reliable results. Also structural models used in those programs are restricted.

In this paper, an accurate structural finite element formulation is established for a bearingless rotor system. Multi-body analysis allows the multiple sub-components to be considered as beam elements respectively.

Geometrically exact beam formulation is used to construct the finite element model to consider nonlinear characteristics precisely and estimate an aeromechanical behavior. The structure model used in the present paper is derived based on the mixed form variational formulation of moving beams suggested by Hodges [8]. Shang implemented this formulation in frequency domain [9] and Cheng [10] further modified it to be implemented in the time domain. Although the linear shape function is used for its integration, more accurate prediction will be obtained by using the present mixed form. By adopting time domain analysis, it can be easily combined with the unsteady aerodynamics.

To enforce the kinematic constraint among the components in the structural model, Lagrange's multiplier is used. In this way, multi-body modeling of the bearingless rotor will be enabled. And further expansion of the present structural model is possible.

2. Structural Model

2.1. Geometrically exact beam formulation

All the outboard main blade, flexbeam, and torque tube are assumed to be an elastic beam.

The three-dimensional, geometrically nonlinear elasticity problem is divided into two dimensional cross-sectional analysis and one dimensional beam analysis. The nonlinear intrinsic beam formulation originally from Hodges [8] assumes small strain and large deformation with finite rotation. By adopting this formulation, analysis of the rotor blade that undergoes large deformation with initial curvature and twist becomes possible without any geometric simplifying approximation.

The variational formulation for a bearingless rotor blade is obtained using Hamilton's principle.

$$\int_{t_1}^{t_2}\int_0^l \left[\delta(K-U)+\delta\overline{W}\right]dx_1 dt = \delta\overline{A} \tag{1}$$

The internal force, internal moment, linear momentum, and angular momentum vectors in the reference frame B in Fig. 2 are introduced as

$$F_B = \left(\frac{\partial U}{\partial \gamma}\right)^T, \quad M_B = \left(\frac{\partial U}{\partial \kappa}\right)^T$$
$$P_B = \left(\frac{\partial K}{\partial V_B}\right)^T, \quad H_B = \left(\frac{\partial K}{\partial \Omega_B}\right)^T \tag{2}$$

In Fig. 2, frame B is a deformed blade reference frame and frame b is an undeformed blade reference frame.

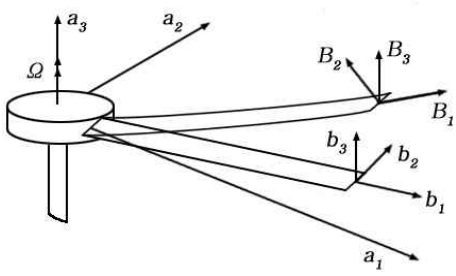

Fig. 2 Coordinate system of beam model

And the deformation and rotation which ensure satisfaction of the geometric exactness are as follows

$$\gamma = C^{Ba}\left(C^{ab}e_1 + u_a'\right) - e_1, \kappa = C^{Ba}\left(\frac{\Delta - \frac{\tilde{\theta}}{2}}{1+\frac{\theta^T\theta}{2}}\right)\theta' \tag{3}$$
$$V_B = C^{Ba}\left(v_a + \dot{u}_a + \tilde{\omega}_a u_a\right), \Omega_B = C^{ba}\left(\frac{\Delta - \frac{\tilde{\theta}}{2}}{1+\frac{\theta^T\theta}{2}}\right)\dot{\theta} + C^{Ba}\omega_a$$

Combining the intrinsic beam formulation with the constitutive and kinematic relationships through the use of Lagrange multipliers, thereby maintaining the generalized displacements, strains, forces, and momenta as independent variables, Eq. (4) is obtained.

$$\begin{aligned}\int_{t_1}^{t_2}\int_0^l \Big[&\delta V_B^* P_B + \delta\Omega_B^{*T} H_B - \delta\gamma^{*T} F_B - \delta\kappa^{*T} M_B \\ &+ \delta F_B^T\left(\gamma-\gamma^*\right) + \delta M_B^T\left(\kappa-\kappa^*\right) - \delta P_B^T\left(V_B - V_B^*\right) \\ &- \delta H_B^T\left(\Omega_B - \Omega_B^*\right)\Big]dx_1 dt + \int_{t_1}^{t_2}\int_0^l \delta\overline{W}\,dx_1 dt = \delta\overline{A}\end{aligned} \tag{4}$$

Transforming the above equation to frame a in Fig. 2 using the rotation matrix and performing

integration by parts, the variational formulation based on exact intrinsic equations for moving beams in the hub rotating frame *a* can be written as

$$\int_{t_1}^{t_2} \delta \Pi_a dt = 0 \tag{5}$$

Through mixed variational formulation, discretized governing equation of each beam is obtained with 18*N*+12 degrees of freedom, which include displacements and rotations, internal forces and moments, linear and angular momenta.

Newton-Raphson method is employed to solve this nonlinear problem. Eq. (6) shows unknown vector of the beam formulation.

$$X = \left[\hat{F}_1^T \hat{M}_1^T \; u_1^T \; \theta_1^T \; F_1^T \; M_1^T \; P_1^T \; H_1^T \right. \\ \left. \cdots u_N^T \; \theta_N^T \; F_N^T \; M_N^T \; P_N^T \; H_N^T \; \hat{u}_{N+1}^T \; \hat{\theta}_{N+1}^T \right]^T \tag{6}$$

where *u* is the displacement vector in the frame *a*, and θ is the rotation vector expressed in terms of the Rodrigues parameters. The hated terms in the above expression are the boundary values of the corresponding quantities that depend on the boundary conditions.

2.2. Kinematic boundary conditions

Fig. 3 shows schematic diagram of a bearingless hub system. Rotor blade, torque tube, and flexbeam are modeled as one-dimensional beam element. Multiple flexbeam can be used depending on the inboard structural configuration. Thus, bearingless rotor is a multi-body system composed of multiple beams.

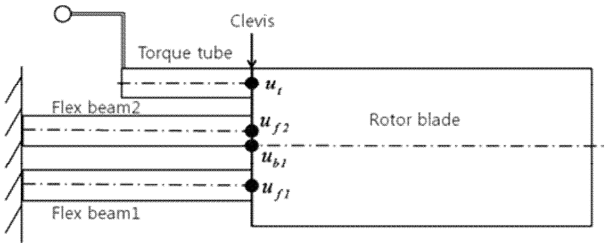

Fig. 3 Schematic diagram of a bearingless rotor

The root of the main blade, the outboard of the flexbeams, and the torque tube are all attached to the clevis. At this point concurrent kinematic constraints exist and these need to be dealt with properly. Due to the relatively large stiffness, the clevis can be assumed to rigid body. Introducing a rigid clevis condition, each beam is perpendicular to the clevis surface at the junction point.

$$\theta_t = \theta_{fi} = \theta_{bl} \qquad at\ clevis \tag{7}$$

where $\theta_t, \theta_{fl}, \theta_{bl}$ are rotation angles due to deflection of a torque tube, flexbeams and a blade, respectively.

And the offsets between each beam at the clevis junction are constant. The displacements of torque tube and flexbeams can be written as

$$u_i = u_{bl} + T_\theta s_i - s_i \qquad at\ clevis \tag{8}$$

where u_i is the displacement vector of torque tube or flexbeam, u_{bl} is the displacement vector of blade, T_θ is the transformation matrix corresponding to the rotation and s_i is the initial offset based on the blade position.

Finally, the cantilevered condition at the flexbeam inboard end is implemented as

$$\begin{aligned} u_{f1} &= \cdots = u_{fN} = 0 \\ \theta_{f1} &= \cdots = \theta_{fN} = 0 \qquad at\ hub \end{aligned} \tag{9}$$

To enforce the kinematic constraint among the components in the structural model, Lagrange's multipliers are used. Total energy of a multi-body system, which consists of multiple beams, is obtained by assembling the energy equations foreach beam.

$$\Pi = \Pi_1 + \cdots + \Pi_{N+2} \tag{10}$$

where *N* is the number of flexbeam. *N*+2 energy equations exist including that of a blade and a torque tube.

And the constraint energy equations related to Lagrange's multipliers is added to Eq. (10)

$$\Pi = \Pi_1 + \cdots + \Pi_{N+2} + \lambda_1 C_1 + \cdots + \lambda_{N+1} C_{N+1} \tag{11}$$

Therefore, the total energy variational equation for the multi-body bearingless rotor as follows

$$\delta\Pi = \delta\Pi_1 + \cdots + \delta\Pi_{N+2} + \sum \lambda \delta C + \sum C \delta\lambda = 0 \tag{12}$$

Similarly, when extra sub-components are added to the rotor system, such as another flexbeam or pitchlink, a revised finite element formulation can be obtained by simply adding individual energy equations to the present equation. In this way, multi-body modeling of the bearingless rotor will be enabled.

2.3. Snubber model

Distinguishing features of the recent bearingless rotors are elastomeric snubber. An elastomeric snubber is placed between the torque tube and the flexbeam in the bearingless rotor.

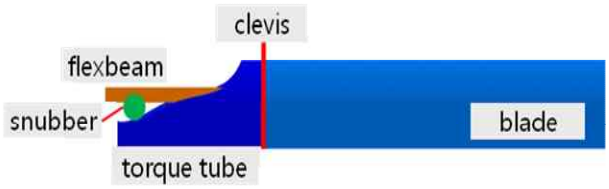

Fig. 4 Snubber model

It can be represented as a combination of a 6-DOF spring and a 6-DOF damper.

The strain energy of a snubber is given by

$$U = \frac{1}{2}\left[\sum k_u (u_t - u_f)^2 + \sum k_\theta (\theta_t - \theta_f)^2\right] \quad (13)$$

And the virtual work done by the snubber damping force is in Eq. (14)

$$\begin{bmatrix} F \\ M \end{bmatrix} = \begin{bmatrix} C_u & \\ & C_\theta \end{bmatrix} \begin{bmatrix} \dot{u}_t - \dot{u}_f \\ \dot{\theta}_t - \dot{\theta}_f \end{bmatrix} \quad (14)$$

These energy terms are added to Eq. (4) and a revised formulation is obtained.

3. Numerical Results

Numerical analysis results are obtained for several bearingless rotor examples.

3.1. Combined 3-beam model

To verify the present combination schemes, test beam analysis is performed. Inboard two beams are connected to the outer blade. And cantilevered boundary condition is enforced to the inboard beams. The material properties of the test beams are described in Table 1.

The results are presented in Fig. 5 compared with the results obtained by DYMORE. A 50N of tip force acting along the Z-direction is considered.

It shows that the displacement compatibility at the connecting point is maintained well and it implies continuity of the bending slope between the beam elements. And the result of the present model is accordance with that by DYMORE.

Table. 1 Material properties of the test beams

Mass per unit span (kg/m)	0.20
I-polar (kg-m)	9.9×10^{-5}
I-theta (kg-m)	1.01×10^{-4}
EA (N)	1.0×10^{6}
EI-flap (Nm^2)	50.0
EI-lag (Nm^2)	1.0×10^{3}
Torsion (Nm^2)	50.0

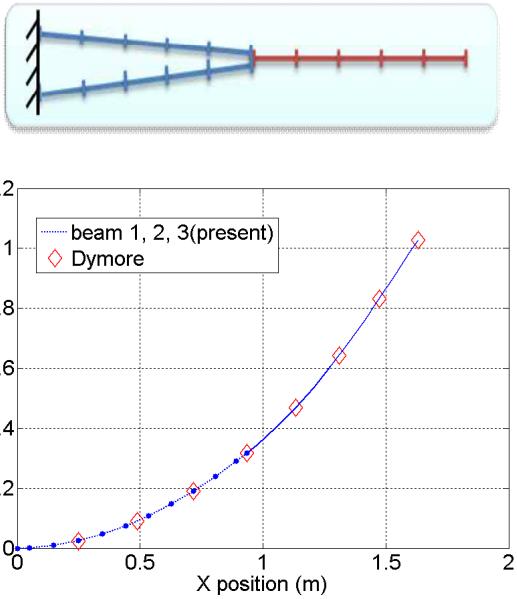

Fig. 5 Displacement comparison result for 3-beam combined bearingless rotor

3.2. BO-105/BMR blade

The BO-105/BMR blade is a bearingless test rotor blade based on the BO-105 hingeless rotor blade [11]. The BO-105/BMR blade configuration is presented in Fig. 6. It adopts inboard two flexbeams. And y-direction offsets of flexbeams with respect to a main blade neutral axis exist. Fig. 7 is the flexbeam stiffness of the test beam.

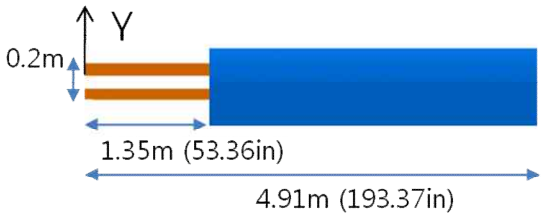

Fig. 6 BO-105/BMR blade configuration

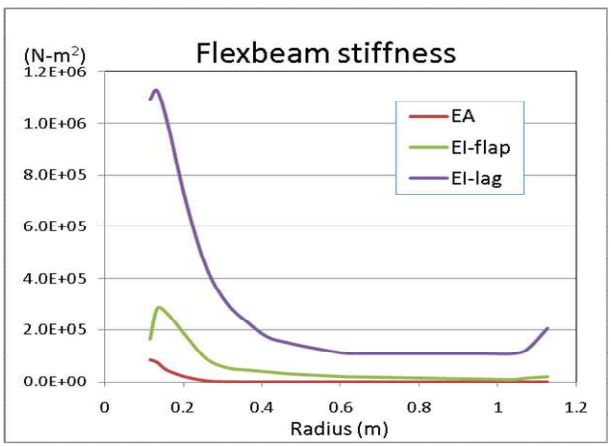

Fig. 7 BO-105/BMR flexbeam stiffness

Figs. 8 and 9 show the comparison of the

displacements under the application of tip force equals to 100 N along with the results from DYMORE simulations. Fig. 8 is a non-rotating case result and Fig. 9 is a rotating one when the rotational speed is 425RPM. It shows the effect of the centrifugal forces applied to the beam elements. It is observed that the two results are generally identical in both cases.

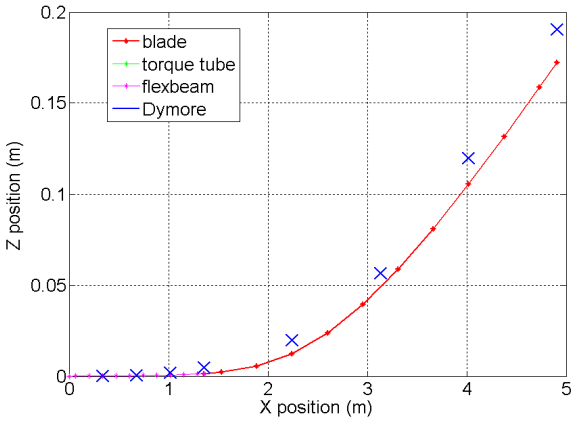

Fig. 8 Deformation of the test blade (Non-rotating)

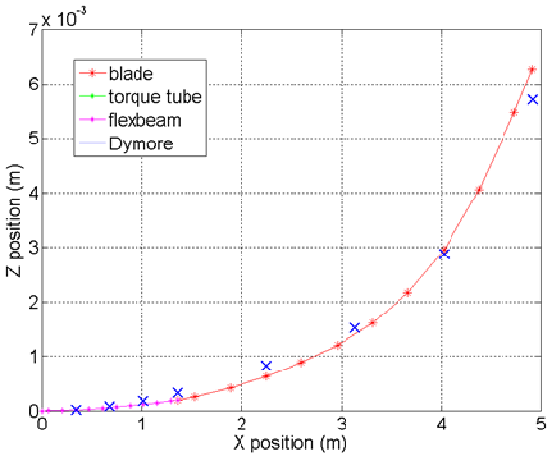

Fig. 9 Deformation of the test blade (Rotating)

3.3. Snubber model

In a snubber model, a torque tube has a floating boundary condition at the inner end. Fig. 10 shows this condition. There exist no constraints through the torque tube, and thus the torque tube will not deform. Also the structural effect of the torque tube upon the other elements is negligible.

When snubber is attached, a torque tube is constrained on both sides as shown in Fig. 11. And a torque tube affects the deformation of the other elements.

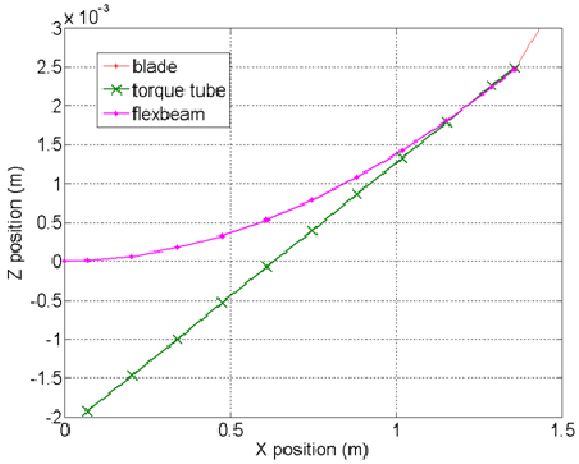

Fig. 11 Inboard displacement of the non-snubber model

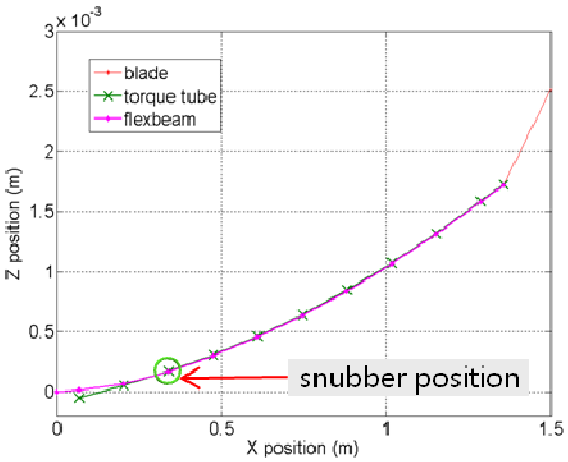

Fig. 121 Inboard displacement of the snubber model

4. Conclusion

A finite-element-based structural analysis has been presented for a bearingless rotor blade. Nonlinear one-dimensional beam formulation satisfying the geometric exactness is derived and practical structural model of a bearingless rotor is presented.

Lagrange's multiplier is used to enforce kinematic constraints among the structural components. In this way, multi-body modeling of a bearingless rotor is produced.

Numerical results show that the present model can be applied to several types of the bearingless rotor systems. The present structural modeling and constraint schemes are verified by comparing results regarding the single and the multiple-combined beam. Also, the analysis results regarding the other types of the bearingless rotor, upon which arbitrary loads and the centrifugal force are applied, are compared with those by

DYMORE.

For further advancement from the present analysis, addition of the damping effects, which is generally due to lead-lag dampers, and addition of the control system such as pitchlink is planned. Cncerning fuselage influences and aerodynamic loads is also planned to conduct in the future.

Acknowledgments

This work was supported by Korea Aerospace Research Institute under Technology Development of Bearingless Main Rotor Hub System funded by the Korea government Ministry of Knowledge Economy

This work is financially supported by Korea Ministry of Land, Transport and Maritime Affairs as 「Haneul Project」

This work was supported by the New and Renewable Energy Program of the Korea Institute of Energy Technology Evaluation and Planning (KETEP) grant funded by the Korea government Ministry of Knowledge Economy (No.20104010100490).

5. Reference

[1] Hodges, D. H., "An Aeromechanical Stability Analysis for Bearingless Rotor Helicopters," Journal of the American Helicopter Society, Vol. 24, No. 1, 1979. pp. 2-9.

[2] Hong, C. H. and Chopra, I., "Aeroelastic Stability Analysis of a Composite Bearingless Rotor Blase," Journal of American Helicopter Society, Vol. 31, No. 4, 1986. pp. 29-35.

[3] Sivaneri, N. T. and Chopra, I., "Finite Element Analysis for Bearingless Rotor Blades Aeroelasticity," Journal of the American Helicopter Society, Vol. 29, No. 2, 1984. pp. 42-51.

[4] Chopra, I., "Dynamic Stability of a Bearingless Circulation Control Rotor Blade in Hover," Journal of the American Helicopter Society, Vol. 30, No. 4, 1985. pp. 40-47.

[5] Bir, G. S. and Chopra, I., "University of Maryland Advanced Rotorcraft Code(UMARC) Theory Manual, Technical Report UM-AERO 94-18," Center for Rotorcraft Education and Research, University of Maryland, College Park, July 1994.

[6] Johnson, W., "Technology Drivers in the Development of CAMRAD II," Proceedings of the AHS Aeromechanics Specialist Conference, AHS International, Alexandria, VA, 1994, pp. 3.1–3.14

[7] Hodges, D. H., and Dowell, E. H., "Nonlinear Equations of Motion for the Elastic Bending and Torsion of Twisted Nonuniform Rotor Blades," NASATN D-7818, Dec. 1974.

[8] Hodges, D. H., "A Mixed Variational Formulation Based on Exact Intrinsic Equations for Dynamics of Moving Beams," International Journal of Solids and Structures, Vol. 26, No. 11, 1990, pp.1253–1273.

[9] Shang, X., "Aeroelastic Stability of Composite Hingeless Rotors with Finite-State Unsteady Aerodynamics," Ph. D. Dissertation, Georgia Institute of Technology, August 1995.

[10] Cheng, T., "Structural Dynamics Modeling of Helicopter Blades for Computational Aeroelasticity," M.S. Thesis, Massachusetts Institute of Technology, May 2002.

[11] Paul H. Mirick, "A Comparison of Theory and Flight Test of the BO 105/BMR in Hover and Forward Flight," Ames Research Center, NASA, Integrated Technology Rotor Methodology Assessment Workshop, 1988, pp. 103-115.